Published in final edited form as:

Cell Rep. 2021 December 07; 37(10): 110095. doi:10.1016/j.celrep.2021.110095.

Stage-specific regulation of DNA methylation by TET enzymes during human cardiac differentiation

Yahui Lan[1], **Kelly M. Banks**[1], **Heng Pan**[2], **Nipun Verma**[3], **Gary R. Dixon**[3], **Ting Zhou**[1,5], **Bo Ding**[4], **Olivier Elemento**[2], **Shuibing Chen**[1], **Danwei Huangfu**[3], **Todd Evans**[1,6,*]

[1]Department of Surgery, Weill Cornell Medical College, New York, NY 10065, USA

[2]Department of Physiology and Biophysics, Englander Institute for Precision Medicine, Institute for Computational Biomedicine, Weill Cornell Medical College, New York, NY 10065, USA

[3]Developmental Biology Program; Memorial Sloan Kettering Cancer Center, New York, NY 10065, USA

[4]Bonacept LLC, 6755 Mira Mesa Blvd, Ste123-360, San Diego, CA 92122, USA

[5]Present address: Memorial Sloan Kettering Cancer Center, New York, NY 10065, USA

[6]Lead contact

SUMMARY

Changes in DNA methylation are associated with normal cardiogenesis, whereas altered methylation patterns can occur in congenital heart disease. Ten-eleven translocation (TET) enzymes oxidize 5-methylcytosine (5mC) and promote locus-specific DNA demethylation. Here, we characterize stage-specific methylation dynamics and the function of TETs during human cardiomyocyte differentiation. Human embryonic stem cells (hESCs) in which all three *TET* genes are inactivated fail to generate cardiomyocytes (CMs), with altered mesoderm patterning and defective cardiac progenitor specification. Genome-wide methylation analysis shows TET knockout causes promoter hypermethylation of genes encoding WNT inhibitors, leading to hyperactivated WNT signaling and defects in cardiac mesoderm patterning. TET activity is also needed to maintain hypomethylated status and expression of *NKX2–5* for subsequent cardiac progenitor specification. Finally, loss of TETs causes a set of cardiac structural genes to fail to be demethylated at the cardiac progenitor stage. Our data demonstrate key roles for TET proteins in controlling methylation dynamics at sequential steps during human cardiac development.

In brief

*Correspondence: tre2003@med.cornell.edu.

AUTHOR CONTRIBUTIONS

T.E. and Y.L. designed the research, interpreted results, and wrote the manuscript. Y.L. performed most of the experiments and bioinformatics analysis. N.V., G.R.D., and D.H. provided mutant hESC lines before publication, along with critical advice. T.Z. and S.C. performed differentiation assays. K.M.B., H.P., B.D., and O.E. assisted for bioinformatics analyses.

DECLARATION OF INTERESTS

The authors declare no competing interests.

SUPPLEMENTAL INFORMATION

Supplemental information can be found online at https://doi.org/10.1016/j.celrep.2021.110095.

Using hESC *in vitro* differentiation and genome-wide methylation analysis, Lan et al. show that TET enzymes fulfill distinct roles at different stages of human cardiomyocyte development. TETs are required to maintain hypomethylation of cardiac regulatory genes and for demethylation of cardiac structural genes.

Graphical Abstract

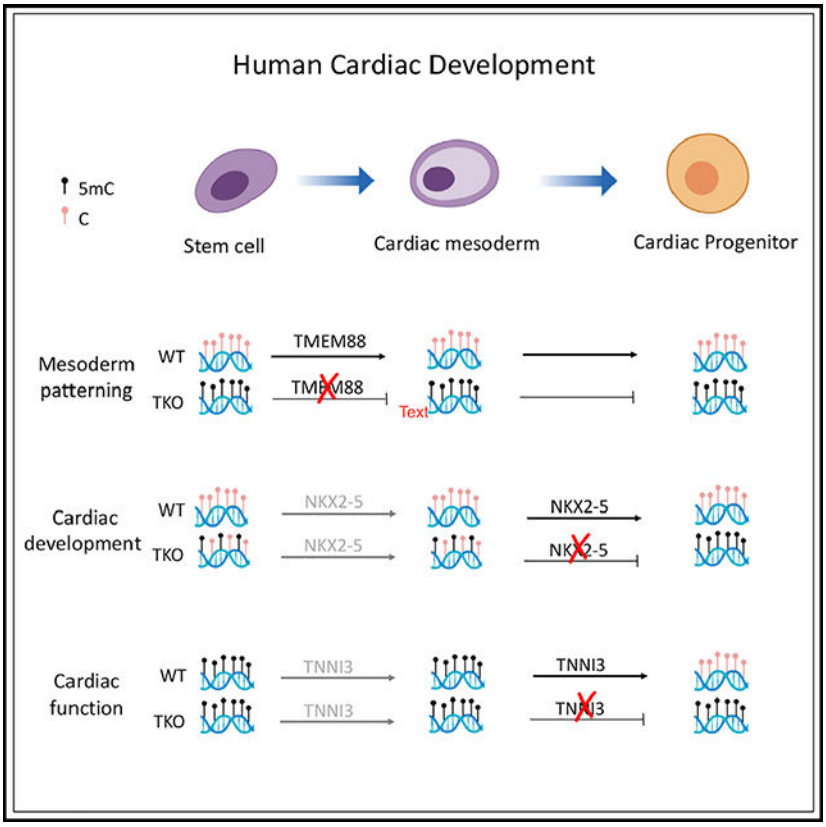

INTRODUCTION

The ability to generate cardiomyocytes (CMs) from human embryonic stem cells (hESCs) or induced pluripotent stem cells (iPSCs) has been useful for studying human cardiogenesis and modeling cardiac disease *in vitro* and provides promise for developing cell-based therapies to treat congenital heart disease (CHD) and adult heart failure. Cardiac development *in vivo* or *in vitro* is exquisitely sensitive to precise temporal regulation of many genes that govern developmental decisions during lineage commitment, including commitment of pluripotent cells to the mesoderm and patterning of the cardiac mesoderm, followed by specification of cardiac progenitors (CPs), and finally to terminally differentiated CMs (Burridge et al., 2015; Evans et al., 2010; Murry and Keller, 2008). In addition to transcription factors, epigenomic regulation, including DNA methylation, histone modifications, and chromation architecture changes, also have important roles in cardiogenesis. For example, epigenomic modifiers, such as the H3K36 methyltransferase WHSC1 (Nimura et al., 2009) and the H3K4 methyltransferase SETD7 (Lee et al., 2018),

control stage-specific gene expression during cardiac differentiation. Large-scale sequencing efforts of CHD parent-offspring trios identified candidate *de novo* causative mutations for numerous genes involved in chromatin modification (Homsy et al., 2015).

Ten-eleven translocation (TET: TET1, TET2, and TET3) proteins catalyze the oxidation of 5-methylcytosine (5mC) to 5-hydroxymethylcytosine (5hmC) and promote active, locus-specific DNA demethylation (Kohli and Zhang, 2013; Wu and Zhang, 2017), regulating DNA methylation and demethylation homeostasis during development (Dawlaty et al., 2014; Koh et al., 2011; Lan et al., 2019; Li et al., 2015a). *Tet* triple-deficient mice exhibit gastrulation patterning defects (Dai et al., 2016), demonstrating a role for TET enzymes in early embryonic development. *Tet2/3* double-knockout mice display an embryonic lethal ventricular non-compaction cardiomyopathy (Fang et al., 2019). 5hmC and 5mC profiles mapped in embryonic, neonatal, adult, and hypertrophic mouse and human CMs indicate dynamic modulation of DNA methylation and hydroxymethylation during heart development and in heart failure (Gilsbach et al., 2018; Greco et al., 2016). However, the mechanisms by which TET enzymes help coordinate complex gene regulatory networks for cardiac differentiation and the specific targets of *de novo* DNA demethylation in establishing cellular identity are undefined. In this study, we systematically investigate DNA methylation dynamics during CM differentiation comparing wild-type (WT) and TET knockout hESCs, which revealed important roles for regulating TET-dependent DNA methylation patterns in cardiac lineage commitment. We identified TET-regulated genes at defined stages of cardiomyocyte development that normally ensure proper cardiac mesoderm (CME) patterning and CP specification.

RESULTS

Differentiation of hESCs toward cardiomyocyte fate is coupled to DNA demethylation in *cis*-regulatory regions of cardiac genes

To study human cardiac development *in vitro*, we carried out directed differentiation of WT hESCs to generate beating CMs, using a chemically defined 14-day protocol (Figure 1A) (Lian et al., 2012). The expression of cardiac-specific genes was evaluated by qPCR and flow cytometry at different developmental stages to ensure proper CM differentiation (Figures S1A and S1B). To evaluate DNA methylation dynamics during CM differentiation, we performed enhanced reduced representation bisulfite sequencing (eRRBS) and focused on four time points: stem cell stage (SC) at day 0, CME at day 3, CP stage at day 8, and beating CMs (>90% $CTNT^+$ cells; Figure S1B) at day 14. During CM differentiation, 3,866 differentially methylated regions (DMRs) that covered 61,653 CpG sites were mapped when cells transitioned from the SC stage to the CM stage (Figure 1B). Notably, nearly all of the DMRs (98%) were defined as hypo-DMRs during the CME to CP transition, whereas the methylation patterns between SC and CME stages and the CP to CM transition were relatively stable. These data are consistent with previous mouse ESC studies suggesting that more than 90% of modified CpGs were hypo-methylated in new CMs compared with that of SCs (Gilsbach et al., 2014) and suggesting an important function for DNA demethylation during human CM differentiation.

Combining these data with published histone marks (Zhang et al., 2019), we determined that hypo-DMRs were mainly located at *cis*-regulatory regions of genes, especially enhancers (54.1%) and promoters (12.96%) (Figure 1C). DNA Genomic Regions Enrichment of Annotations Tool (GREAT) analysis of hypo-DMRs revealed that these regions are enriched at genes essential for embryonic development and cardiac morphogenesis (Figure 1D), such as *GATA5* and *TNNI3* (Figures 1E and S1C). Motif analysis demonstrated hypo-DMR regions were enriched for DNA sequences with known motifs for binding by key cardiac transcription factors, including GATA4, GATA6, FOXP1 and MEF2C (Figure 1E), suggesting a close link between DNA demethylation and cardiac development.

Interestingly, when we investigated the methylation status of key cardiac regulatory genes, we found differences comparing promoters and enhancers. Most of these genes retain hypomethylated status in their promoter regions throughout all stages of CM differentiation, even before being marked by H3K27Ac (representative example shown for *GATA5* in Figure 1E; others shown in Figure S1D), implying a mechanism that primarily restricts methylation, rather than promoting active demethylation at these promoters. Hypo-DMRs located in enhancer regions were highly enriched for programs of cardiac development, such as myotube differentiation and cardiac chamber morphogenesis (again true for *GATA5* in Figure 1E; GREAT analysis is in Figure S1E), suggesting that DNA demethylation mainly occurred in the distal regulatory regions of early cardiac developmental genes. In contrast, hypo-DMRs mapping to promoter regions were related to genes for muscle contraction and cardiomyocyte function (representative examples shown for *TNNI3* in Figure S1C; others shown in Figure S1F). Taken together, the epigenomic analysis validated that DNA demethylation is closely associated with cardiac development and CM differentiation and occurs at different genomic regions for cardiac developmental genes (at enhancers) compared with structural genes (at promoters). (Note that a broader meta-analysis of global methylation in WT cells compared with TET mutant cells is presented in Figure 4).

Loss of TETs impairs human cardiac differentiation

A major function of TET enzymes is performing active DNA demethylation (Kohli and Zhang, 2013; Wu and Zhang, 2017). To further probe the significance of the observed *de novo* DNA demethylation in directing hESCs toward a CM fate, CM-directed differentiation was performed using a panel of *TET* knockout lines. No significant CM differentiation defect was observed using isogenic *TET2*, *TET3*, or *TET2/3* double-knockout lines (Figure 2A). In contrast, the *TET1* knockout line displayed a significant decrease in its capacity to generate $CTNT^+$ CMs. Moreover, hESCs in which all three *TET* genes were inactivated (TET triple-knockout [TKO] hESCs) failed entirely to generate CMs. Using TET TKO hESCs in which one mutated *TET1* allele was reverted to the WT sequence through CRISPR-Cas9-mediated homology-directed repair (TKO-TET1r), CM differentiation was effectively rescued (Figure 2A). Notably, of the three *TET* genes, *TET1* showed the greatest transcript levels in hESCs and in early CM differentiation stages (Figure 2B). Therefore, TET expression, especially TET1, is necessary for CM differentiation.

Differentiation using TET TKO cells with a distinct hESC parental background (MEL-1), confirmed that TETs are required for CM generation (Figure S2A). Stage-specific

cardiac gene expression was compared in WT and TKO lines at different stages of CM differentiation. Consistent with previous findings (Verma et al., 2018), TET TKO hESCs showed no statistically significant difference in expression of pluripotency markers compared with WT hESCs (Figure S2B). RNA sequencing (RNA-seq) profiles suggested that TKO hESCs expressed transcripts for differentiation genes (Gene Ontology [GO] analysis in Figure S2C), including mesendoderm markers *T* and *SOX17*, which was further demonstrated by qPCR as well as immunostaining (Figures S2D and S2E), suggesting that TKO hESCs might be primed for differentiation, especially to mesendoderm. Indeed, TKO hESCs differentiated to mesendoderm more efficiently compared with WT hESCs at day 1, indicated by the greater expression level of mesendoderm markers *MIXL1* and T (Figures S2F and S2G), consistent with a previous study showing that *Tet1/2/3*-deficient mouse ESCs showed impaired neuroectodermal development, with a skewed bias toward mesoderm fate (Li et al., 2016). The TKO cells were not biased to endoderm because they were relatively less efficient then WT cells at forming activin-induced endoderm (not shown). At day 3, the differentiating TKO cells expressed somewhat lesser levels of CME markers *ISL1* and *GATA4* (Figures 2C and 2E), as well as a modest decrease in numbers of kinase insert domain receptor-positive/platelet-derived growth factor subunit A-positive ($KDR^+/PDGFRA^+$) progenitor cells (Figure 2F). However, compared with WT cells, CP genes, including *TBX5*, *NKX2–5*, and *MYH6* failed to be expressed at day 6 in TKO cells (Figures 2D and 2E). Flow cytometry revealed that WT cells partitioned into distinct populations, including $KDR^{low}/PDGFRa^+$ CPs and a small population of $KDR^{high}/PDGFRa^-$ cardiovascular progenitors at day 6, consistent with previous single-cell-sequencing data (Friedman et al., 2018). In contrast, most TKO cells remained phenotypically $KDR^{high}/PDGFRa^+$ (Figure 2F), suggesting that TKO cells are blocked in the capacity to specify CPs. These data show that early mesoderm development is independent of TET function but that TETs are required for CP specification and differentiation.

Dynamic regulation of methylation through TET enzymes during CM differentiation

To dissect the underlying molecular defects caused by the lack of TET proteins, we also performed eRRBS in TET TKO cells at the same stages as WT cells (SC, CME, and CP; note that TKO cells can not generate beating CMs, so eRRBS was not performed with day-14 TKO cells). Consistent with previous human and mouse ESC data (Dawlaty et al., 2014; Verma et al., 2018), loss of *TETs* resulted in locus-specific hyper-methylation in hESCs. We identified 7,593 hyper-DMRs and only 139 hypo-DMRs in TKO ESCs compared with WT ESCs (Figure 3A). In contrast to WT cells, which, during differentiation, underwent DNA demethylation, TKO cells showed methylation increases during CM differentiation. From SC to CP stages, 2,075 DMRs were mapped, and just 323 were identified as hypo-DMRs (Figure 3B). Moreover, 1,496 DMRs were defined as hyper-DMRs during the CME to CP transition (Figure 3B). As a result, by the CP stage, the number of hyper-DMRs accumulated in the TKO cells had nearly doubled compared with that of the SC stage (14,000) (Figure 3A). Although there remains a small set of hypo-DMRs during the TKO differentiation (Figure 3B), they are not overlapped with hypo-DMRs found during WT CM differentiation (Figure S3A), and these TKO hypo-DMRs were not enriched for any functional category. They could form as a direct consequence of *TET* inactivation or

by a secondary effect, for example, redirection of DNA methyltransferases (DNMTs) in TKO cells. In contrast, GREAT analysis showed that TKO hyper-DMRs were enriched at genes closely associated with embryonic organ and heart development (Figure 3C). These data demonstrate that *de novo* DNA demethylation was markedly blocked during TKO differentiation, which might underlie the cardiac developmental defect.

To determine whether methylation changes in TKO cells are the direct consequence of TET knockout, we used a previously described *TET1*-V5 endogenously tagged line (Dixon et al., 2021) and performed TET1-V5 chromatin immunoprecipitation sequencing (ChIP-seq) in cardiac progenitors to compare binding sites mapped in pluripotent stem cells. In SCs, we observed considerable overlap between hyper-DMRs formed in the TKO cells with TET1 occupancy in WT cells, with 92% of hyper-DMRs overlapping with TET1 peaks (Figure 3D), and with the WT TET1 peaks and TKO hyper-DMRs sharing similar genomic features (Figure S3B). Similarly, we observed 80% overlap between TKO cell hyper-DMRs and WT TET1 peaks in CPs (Figure 3E) with similar genomic features (Figure S3C), supporting the hypothesis that loss of the TET proteins is directly responsible for gain of methylation in TKO cells. We next compared during WT cell differentiation the TET1 peaks identified in SCs and CPs and identified 33,049 common peaks, 14,173 SC-specific peaks, and 12,867 CP-specific peaks (Figure 3F). GREAT analysis showed that the SC-specific peaks were enriched for terms of neuron fate commitment, timing of cell differentiation, and stem cell maintenance (Figure S3D). Surprisingly, the CP-specific peaks were enriched for terms of cell metabolic process, regulation of gene silencing, and cellular biosynthetic process but not cardiac-specific lineage terms (Figure S3E). In fact, although in WT cells 80.2% of hypo-DMRs identified in the CME to CP transition overlapped with TET1 peaks at the CP stage, only 18.4% of them overlapped with TET1 CP-specific peaks (Figure S3F), suggesting that most demethylated regions are already occupied by TET1 at the SC stage. During cardiac development, TET1 binding is decreased in lineage-specific factors for non-cardiac lineages, such as early development (*T*) and neuronal cell fate (*PAX6)* (Figure S3G). For cardiac-specific factors, such as *GATA5* and *TNNI3*, we found consistent TET1 binding throughout SC to CP stages, regardless of whether the region normally undergoes DNA demethylation (as for *TNNI3*) or not (for example, *GATA5*) (Figures 3G and 3H).

Distinct methylation signatures for different categories of cardiac factors

Because the methylation status of promoters often correlates with expression, we focused first on promoter regions and comprehensively compared methylation patterns around transcription start sites (TSSs) during each stage of CM differentiation in both WT and TKO cells. A total of 1,074 genes displayed significant promoter methylation changes in at least one of the six defined conditions (WT or TKO cells at the SC, CME, or CP stage) and were categorized as four groups with distinct methylation patterns (Figure 4A; Table S1). Genes in group I showed DNA demethylation during CM differentiation of WT cells and included genes related to terminal differentiation, such as for muscle contraction and calcium regulation. This loss of methylation failed during differentiation of TKO cells. In contrast, genes in groups II, III, and IV displayed relatively stable low-methylation levels throughout differentiation of WT cells. However, in TKO cells, they showed distinct hyper-methylation defects. The group II genes showed a consistent and severe hyper-methylation

throughout differentiation of TKO cells, from SC to CP stages, and were enriched for genes associated with plasma membrane and basic biological processes. Genes in group III, including genes for early pattern specification and development, displayed mild hyper-methylation in TKO cells during differentiation. The genes in group IV showed moderate hyper-methylation in TKO SCs and underwent further hyper-methylation during progression to the CP stage. Notably, genes in group IV included many cardiac developmental regulatory genes, including *NKX2–5*, *GATA5*, and *WT1*. These groups represent progressive stages of cardiac development and are consistent with the phenotype of TKO cells in which cardiac mesoderm was partially affected but cardiac progenitor specification was entirely blocked.

We next evaluated whether specific chromatin marks were associated with expression patterns characteristic for each group of genes, with a special interest in group I and group IV classes because they showed dynamic methylation changes during differentiation of WT or TKO cells, respectively, and are enriched for genes associated with cardiac development and function. In WT cells at the SC stage, most genes in group I were marked as “silent” promoters (the absence of H3K4me3) (Figure S4A), yet the expression levels of those genes were significantly lower in TKO cells (Figure 4B), consistent with previous evidence that hyper-methylation of silent promoters is associated with a decrease in gene-expression levels (Verma et al., 2018). In contrast, in WT cells at the SC stage, most of group IV genes displayed a bivalent promoter signature (marked by H3K4me3 and H3K27me3) (Figure S4A) and were not differentially expressed (Figure 4B). Notably, during CM differentiation, transcript levels in TKO cells for genes in both group I and group IV were significantly lower at the CP stage compared with stage-matched WT cells (Figure 4B). Interestingly, during differentiation of WT cells, the group-IV cardiac regulatory genes displayed high levels of H3K27me3 at the SC stage, which gradually decreased as differentiation progressed. In contrast, the group-I genes encoding contractile proteins were not marked by appreciable levels of H3K27me3 at the SC stage but showed significantly increased levels of H3K4me3 during differentiation (Figures 4C and S4B). This correlates with the fact that cardiac regulatory genes (group IV) maintained low DNA methylation levels at all stages of differentiation, whereas cardiac functional genes (group I) undergo DNA demethylation during differentiation. This suggests that, although genes encoding cardiac regulatory factors and cardiomyocyte contractile proteins both show time-dependent increases in RNA expression (Figure 4C), they depend on different mechanisms to ensure gene expression at the appropriate developmental stage.

In addition to promoters, dynamic methylation changes were also mapped at enhancer regions. Active enhancer regions at the CP stage were annotated based on the histone mark H3K27ac (Zhang et al., 2019), and methylation status was determined (Figure S4C). As shown above, during differentiation of WT cells, DNA demethylation occurs at distal enhancers of cardiac regulatory genes. Consistent with that data, a set of enhancers was identified, enriched for circulatory system development and cardiac morphogenesis, which underwent DNA demethylation during WT differentiation but failed to do so during TKO differentiation (Figure S4C), consistent with TET-dependent demethylation, primarily at the CME to CP transition. Interestingly, enhancers for calcium ion homeostasis and muscle function were consistently hypo-methylated during both WT and TKO differentiation (Figure S4C), suggesting this group is regulated independent of TET function. Therefore,

TETs are required for active demethylation (in enhancer regions of cardiac developmental genes and promoter regions of cardiac functional genes) and are also necessary to maintain hypo-methylated status (in the promoters of cardiac developmental genes) to ensure proper cardiac lineage commitment.

TETs control mesoderm patterning by influencing the methylation and expression of genes encoding WNT inhibitors

To identify genes that mediate TET function for commitment to cardiac mesoderm fate, transcript profiling was performed by RNA-seq analysis at day 3, just before the CME specification stage. GO analysis (Figure S5A) for genes with relative decreased levels of expression in TKO-derived cells highlighted early cardiac differentiation pathways, including heart morphogenesis and endocardial cushion morphogenesis. Upregulated genes in TKO-derived cells were associated with primary germ layer formation, including endoderm (Figure S5A). Notably, genes associated with embryonic skeletal or kidney development were also increased significantly in TKO-derived cells (Figure S5A). During development, early mesoderm segregates into paraxial mesoderm (PM; including progenitors for somites), intermediate mesoderm (IM; including progenitors for kidney), and lateral mesoderm (LM; including progenitors for heart and extraembryonic mesoderm). Therefore, expression levels were evaluated for key regulatory genes of distinct mesoderm subtypes at day 2, the mesoderm patterning stage. In TKO cells, mRNA expression levels of the LM marker genes *ISL1* and *HAND1* were significantly down, whereas those for PM marker genes *CDX2* and *MSGN1*, and IM marker gene *PAX2* showed a significant increase (Figure 5A). This skewed gene expression pattern was validated at the protein level by immunostaining of ISL1 and PAX2 (Figure S5B; WT compared with TKO), demonstrating a mesoderm patterning alteration in TKO-derived cells.

To investigate the specific mechanism by which TETs regulate mesoderm patterning, pathway analysis was performed with transcript profiles obtained by RNA-seq at day 3, which showed that TKO cells display greater WNT signaling activity (Figure S5C). During mesoderm patterning, higher WNT levels posteriorize LM and promote PM and IM specification (Lam et al., 2014; Loh et al., 2016). We tested whether early mesoderm in differentiating TKO cells was skewed toward PM and IM at the expense of LM because of hyperactive WNT signaling by performing luciferase assays with a WNT reporter (Figure 5B) and by western blotting to measure active β-catenin (Figure 5C). In stem cells, before differentiation, both WT and TKO cells displayed relatively low WNT activity. Using the standard CM differentiation protocol, following addition of the GSK3-β inhibitor CHIR to activate WNT and induce mesoderm, WNT activity was slightly greater at day 1, (Figure 5B), consistent with enhanced expression of early mesoderm markers (Figures S2F and S2G). At day 2, the TKO cells maintained relatively hyperactive WNT signaling compared to WT cells, according to both WNT reporter luciferase assays and western blotting for activated β-catenin (Figures 5B and 5C).

To investigate whether enhanced WNT signaling is the reason for the LM formation defect in TKO cells, WNT inhibitor IWP2 was added at the end of day 1, which effectively lessened WNT signaling in both WT and TKO cells on day 2 (Figures 5B and 5C). Notably,

inhibiting WNT signaling reversed the skewed differentiation of TET TKO mesoderm cells, indicated by enhanced expression levels for the LM marker genes *ISL1* and *HAND1*, and relative reduction of the PM and IM marker genes *CDX2*, *MSGN1*, and *PAX2* (Figures 5A and S5B). If, instead of inhibiting WNT, we maintained exposure to CHIR through day 2, LM formation was limited in both WT and TKO cells and induced expression of PM and IM markers more efficiently in TKO cells compared with WT cells (Figure S5E), showing that TETs are not required for differentiation to PM and IM.

Previous studies suggested that TETs can inhibit WNT signaling through demethylation of promoters of genes encoding WNT inhibitors in the context of mouse neuroectodermal and mesodermal fate choice (Li et al., 2016) and in nasopharyngeal carcinoma (Fan et al., 2018). Because the mesoderm patterning defect in TKO cells occurred at a stage before WT cells underwent significant demethylation, we analyzed promoters that already showed relative hyper-methylation in TKO cells at the SC stage. Pathway analysis revealed that these hyper-DMR-associated genes were enriched for several signaling pathways, including WNT signaling (Figure 5D). Combining RNA-seq and eRRBS data, we identified 21 genes with hyper-methylated promoters that can negatively regulate the WNT pathway (Table 1). Within that gene set, almost all (20 of 21) were upregulated for expression levels in WT cells at the CME and CP stages during CM differentiation and more than half (13 of 21) had significant reductions in gene expression levels at these stages in TKO cells (Figure 5E).

Among these hyper-methylated and downregulated genes, TMEM88 is of particular interest. We and others previously identified TMEM88 as required during cardiac progenitor specification both during zebrafish development and during CM differentiation from hESCs (Novikov and Evans, 2013; Palpant et al., 2013). More recently, we showed TMEM88 functions as an inhibitor of WNT signaling by promoting WNT signalosome localization to multivesicular bodies (Lee and Evans, 2019). Promoter hyper-methylation of *TMEM88* has been found in cancer and correlated to low mRNA expression and shorter overall survival (Ma et al., 2017). In TET TKO cells, eRRBS data showed a severe hyper-methylation of the promoter and associated upstream regions of *TMEM88* in TKO cells from SC through CP stages (Figure 5F), which was also confirmed by PCR-based bisulfite sequencing (Figure S5D). We also detected strong TET1-V5 binding at the *TMEM88* promoter in WT SCs as well as CPs by ChIP-seq (Figure 5F), and this was also validated by ChIP-qPCR (Figure S5E).

To confirm that failure of *TMEM88* activation in TKO cells was due to hyper-methylation of the *TMEM88* gene, a targeted demethylation strategy was used, with a TET1 catalytic domain fused to a nuclease “dead” Cas9 (dCas9) in combination with guide RNAs (gRNAs) specifically targeting the *TMEM88* promoter. A lentiviral vector was used to express dCas9-TET1 protein (and EGFP) and a second lentiviral vector with an mCherry reporter to express three gRNAs targeting the *TMEM88* promoter. After sequential infection and fluorescence-activated cell sorting (FACS) to purify double-transduced cells, TKO and TKO-transduced ESCs were differentiated. Subsequent PCR-based bisulfite sequencing showed a consistent, albeit partial, rescue of the hypermethylation phenotype across the *TMEM88* promoter of TKO cells after introduction of gRNAs/dCas9-TET1 (Figure S5D). The qPCR analysis confirmed that *TMEM88* fails to be upregulated at day 2 in TKO cells, whereas levels are

significantly increased in TKO cells expressing gRNAs and dCas9-TET1 (Figure 5G). Taken together, our data demonstrate that TET activity modulates WNT signaling levels required for proper mesoderm patterning through modifying methylation status of WNT inhibitory genes, including *TMEM88*.

TETs regulate key cardiac progenitor specification gene *NKX2–5*

We tested whether manipulating WNT signaling to restore normal mesoderm patterning was sufficient to rescue CM differentiation. Indeed, using the modified protocol by adding the WNT inhibitor IWP2 from the end of day 1, cardiac mesoderm was successfully generated with the TET TKO line, indicated by normal expression levels at day 4 for CME markers *ISL1* and *GATA4* (Figure S6A), as well as equivalent populations of KDR^{+}/$PDGFRA^{+}$ progenitor cells (Figure S6B). However, subsequent cardiac development failed because *ISL1* and *GATA4* transcript levels were not maintained relative to WT cells. RNA-seq analysis at day 6 revealed downregulation of cardiac-related processes in TKO cells, including cardiac muscle cell differentiation and sarcomere organization (Figure S6C). qPCR analysis validated that, at day 6, CP genes, including *NKX2–5* and *MYH6*, failed to be expressed in TKO cells (Figure S6A). Flow cytometry revealed that WT cells partitioned into distinct populations, including KDR^{low}/$PDGFRa^{+}$ CPs and a small population of KDR^{high}/$PDGFRa^{-}$ cardiovascular progenitors at day 6, yet most TKO cells remained phenotypically KDR^{+}/$PDGFRa^{+}$ (Figure S6B), and they do not express cardiac markers, suggesting a block in the capacity to specify CPs. As a result, TET TKO cells still failed to differentiate to CMs (Figure S6D).

The effect on *NKX2–5* was further analyzed because it is a key marker for CP specification and failed to be upregulated during TKO cell differentiation (Figure S6A). Indeed, *NKX2–5* is a group-IV gene that displays hyper-methylation at the TKO SC stage and is further methylated during TKO differentiation, with strong TET1-V5 binding in WT stem cells as well as CPs, demonstrated by ChIP-seq (Figure 6A) and validated by ChIP-qPCR (Figure S5E). A rescue experiment was performed using an *NKX2–5* transgene under the control of a doxycycline-inducible promoter in TKO cells during CM differentiation. TKO cells exposed to doxycycline from day 4 to day 6 expressed *NKX2–5* mRNA and protein (Figures S7A and S7B), which partially rescued the CM differentiation block in TKO cells, shown by restored transcript levels of cardiac markers *TBX5* and *CTNT* (Figure S7B). Moreover, although we can not claim these CMs are entirely normal, flow cytometry revealed a partial rescue of $CTNT^{+}$ CMs in TKO cells expressing *NKX2–5* (Figure 6B). Interestingly, overexpression of *NKX2–5* in WT cells reduced CM differentiation efficiency (Figure 6B), demonstrating that expression levels of *NKX2–5* need to be strictly regulated during cardiac development.

To confirm that failure of *NKX2–5* activation in TKO cells was due to hyper-methylation of the *NKX2–5* gene, a similar demethylation strategy was used with a TET1 catalytic domain fused to a nuclease “dead” Cas9 (dCas9) in combination with guide RNAs (gRNAs) targeting specifically the *NKX2–5* promoter. The TKO cells expressing gRNAs and dCas9-TET1 were partially rescued for the hypermethylation phenotype consistently throughout the *NKX2–5* promoter (Figure S7C). These cells express *NKX2–5* mRNA and protein at the

CP stage (Figures 6C and 6D). However, cells expressing gRNAs and a mutant version of dCas9-TET1, in which the TET1 catalytic domain was inactivated, were unable to activate the *NKX2–5* gene.

Finally, given that the promoter of *NKX2–5* was already hyper-methylated in TKO cells at the SC stage, we tested whether TET expression at the SC stage would be sufficient to rescue the later developmental defect. For this purpose, TKO ESCs were infected with a lentiviral vector expressing TET1 under doxycycline control, and CM-directed differentiation was performed with doxycycline treatment within defined time windows (Figure S7D). When TET1 expression was induced at the SC stage and throughout differentiation, qPCR and immunostaining analyses demonstrated efficient rescue of *NKX2–5* expression. This was the case regardless of whether TET1 expression was induced before or at the time of initiating differentiation. In contrast, induction of TET1 expression only at the SC stage, with doxycycline removed during differentiation, was unable to rescue *NKX2–5* expression (Figures 6E and 6F).

DISCUSSION

During CM differentiation, most CpGs were hypo-methylated rather than hyper-methylated in CMs compared with SCs. In contrast, comparative analysis of prenatal development and postnatal CM maturation found both hypo-methylated and hyper-methylated genes (Gilsbach et al., 2014, 2018), with loss of mCpG associated with increased expression of genes essential for myofibril structures and regulation of contraction. Increased mCpG was linked to decreased gene expression of primarily developmental genes. Notably, no genes with opposing mCpG changes during prenatal versus postnatal life were identified (Gilsbach et al., 2014, 2018). These data support an interpretation that DNA demethylation is important early to activate lineage specific genes during embryonic development, whereas DNA methylation serves as a one-way, permanent, inhibitory mechanism to silence early developmental genes at later stages during differentiation.

We used *TET* TKO hESCs to completely block TET activity because dissecting functions of distinct *TET* genes may be complicated by compensation. For single genes, knockout of *TET1* caused a partial loss of CM fate, which was not seen for either *TET2* or *TET3* mutant lines. This may simply reflect the fact that TET1 is highly expressed in ESCs, whereas TET2 and TET3 are expressed at very low levels in hESCs and mESCs, respectively (Koh et al., 2011; Langlois et al., 2014; Li et al., 2018). In mouse embryos, *Tet1* functions at an early postimplantation stage, when paralogs *Tet2* and *Tet3* are not detectably expressed (Khoueiry et al., 2017). The *TET1* knockout hESCs were shown previously to fail differentiation into neuroectoderm cells because TET1 normally binds at the *PAX6* promoter to prevent hyper-methylation, thus ensuring robust lineage-specific transcription upon neural differentiation (Verma et al., 2018). Likewise, in murine ESCs TET1 and polycomb repressive complex 2 (PRC2), which is responsible for H3K27 methylation, are recruited together to maintain a hypo-methylated state at bivalent promoters with known developmental functions (Wu et al., 2011). Therefore, a key function of TET1 at the SC stage is to maintain hypo-methylated states at promoters that are, at that time, repressed because they are enriched for both H3K4me3 and H3K27me3. Upon differentiation, H3K27me3 can be readily removed and

the hypo-methylated promoters are available for immediate response to lineage-driving transcription factors. This mechanism ensures flexible, yet rapid, transcriptional regulation during early development.

TET2 and TET3 are expressed at higher levels in differentiated cells. TET3 expression levels increased significantly in hESC-derived neuroectoderm and pancreatic endoderm (Li et al., 2018; Li et al., 2015b), whereas TET2 is widely expressed in multiple somatic cell types, including hematopoietic cells (Kunimoto et al., 2012; Langlois et al., 2014; Moran-Crusio et al., 2011) and is the most highly expressed paralog in fetal murine CMs (Fang et al., 2019). Cardiac-specific loss of *Tet2* and *Tet3* in mice causes ventricular non-compaction cardiomyopathy (NCC) with embryonic lethality, whereas knockdown of *Tet2* in embryonic CMs affected the expression of key cardiac structural genes, such as *Myh7* and *Myl4* (Fang et al., 2019). In our experiments using human ESC-derivatives, *TET2* was strikingly upregulated during CM differentiation, although *TET2* knockout alone did not affect CM differentiation efficiency. Because the promoters of cardiac structural genes undergo demethylation during CM differentiation, *TET2* seems likely to be functional at these later stages, perhaps compensated in the *TET2* knockout hESCs by redundant functions of TET1/3. Although the genes are highly conserved across vertebrate species, specific genes may be used differently in human cells compared with animal models. For example, early embryonic zebrafish do not express *tet1* at high levels (Almeida et al., 2012), and zebrafish *tet2/3* double-mutant embryos, essentially devoid of 5hmC, show no defect in CM specification and only develop later cardiac defects related to atrial ventricular canal and epicardial development (Lan et al., 2019). In summary, our integrative genomic and epigenomic analyses provide an atlas of DNA methylomes representative of key stages of *in vitro* human CM differentiation. They reveal previously unrecognized roles of TET activity in human cardiac development and identify key target genes at each stage of CM differentiation.

Limitations of the study

Our study focused on early developmental stages, whereas TET enzymes, especially TET2, are implicated in pathogenesis of cardiovascular disease (CVD) at later stages (Zadeh et al., 2020). Conditional knockout alleles will be helpful to study the function of TETs during cardiomyocyte maturation. Given the emerging effect recognized for altered epigenomics in cardiovascular disease (Zadeh et al., 2020), a detailed understanding of the epigenomic regulatory mechanisms underlying human cardiogenesis may provide fundamental insights into the etiology of heart defects.

STAR★METHODS

RESOURCE AVAILABILITY

Lead contact—Further information and requests for reagents should be directed to and will be fulfilled by Todd Evans (tre2003@med.cornell.edu).

Materials availability—Plasmids generated in this study are available from the lead contact upon request. The modified hESC lines are available from the lead contact upon request under a material transfer agreement.

Data and code availability

- Sequencing data are available at GEO and are publicly available as of the date of publication. The series accession number is GEO: GSE186848.
- Any additional information required to reanalyze the data reported in this paper is available from the lead contact upon request.

EXPERIMENTAL MODEL AND SUBJECT DETAILS

hESC lines and culture condition—The HUES8 (NIHhESC-09–0021, male) and MEL-1 (NIHhESC-11–0139, male) hESCs with TET mutations, and TET-TKO line in which one allele of TET1 was repaired (TKO-TET1r) have been described (Verma et al., 2018). The TET1-V5 line (H1 NIHhESC-10–0043, male, with a V5 epitope tag inserted at the C terminus of the endogenous TET1 protein sequence) has been described (Dixon et al., 2021). All hESCs were cultured on Matrigel-coated plates (BD Biosciences) in mTesR1 Medium (STEMCELL Technologies) at 37°C. The medium was changed daily.

METHOD DETAILS

Differentiation of human hESCs to CMs—For cardiac differentiation, a chemically defined monolayer differentiation protocol was used as previously described (Lian et al., 2012). Briefly, hESCs at 40% confluence were incubated with differentiation basal medium comprising RPMI 1640 medium (Invitrogen) and B27 supplement minus insulin (Invitrogen). 6 μM CHIR99021 was added to the differentiation basal medium. On day 2, medium was removed and replaced with differentiation basal medium minus CHIR99021. On day 3, 5 μM IWP2, the Wnt antagonist, was added to the medium. In a modified protocol, IWP2 was added on day 1 instead of day 2. On day 5, medium was removed and replaced with differentiation basal medium without any inhibitors. On day 7, the cells were incubated with complete CM medium consisting of RPMI 1640 medium and B27 supplement plus insulin (Invitrogen). The medium was changed every 2 days. At day 9 cells were incubated with cardiac enrichment medium (RPMI 1640 without glucose (Life technologies) + 4 mM sodium L-lactate (Sigma-Aldrich). Cells were kept in enrichment medium for 3 days. After enrichment phase medium was switched back to complete CM medium (RPMI + B27).

Differentiation of human hESCs to endoderm—To differentiate hESCs to endoderm, the hESCs were first differentiated in RPMI 1640 medium (Invitrogen) and B27 supplement minus insulin (Invitrogen) supplemented with 6 μM CHIR99021 for 24 hr, and further differentiated in the presence of 25ng/mL human recombinant Activin A (R&D Systems) for 48 hr.

RNA extraction and quantitative RT-PCR—Total RNA was isolated with the RNeasy Mini kit (QIAGEN). RNA was reverse transcribed with the Superscript III First-Strand

Synthesis System (Invitrogen). The qPCR analysis was performed on a LightCycler 480 II (Roche) using LightCycler 480 Sybr Green master mix (Roche). Primer sequences are provided in Table S2. Relative mRNA levels were normalized to those of HPRT mRNA in each reaction. At least three biological replicates per group were used for qRT-PCR.

Western blotting—Whole cell extracts were collected in RIPA lysis buffer (Millipore) in the presence of Protease/Phosphatase inhibitor (Cell Signaling, Danvers, MA). Proteins were resolved by electrophoresis on 10% NuPage Bis-Tris gels (Invitrogen) and transferred to poly (vinylidene difluoride) membranes (Bio-Rad, Hercules, CA). Membranes were blocked in 5% IgG-free BSA and probed overnight with antibodies. Antibodies used are listed in the Key resources table. Proteins were visualized with horseradish peroxidase-conjugated secondary antibodies (Bio-Rad).

Immunostaining—Cells were fixed in tissue culture dishes with 4% paraformaldehyde (PFA) at room temperature (RT) for 20 minutes. They were blocked for an hour in phosphate-buffered saline (PBS) supplemented with 10% FBS, 0.1% IgG-free BSA (Jackson ImmunoResearch, West Grove, PA) and 0.1% saponin (Sigma) at RT. Cells were incubated with primary antibody overnight at 4°C in blocking buffer. Fluorescence-conjugated secondary antibody was used for visualization. Antibodies used are listed in the Key resources table. Nuclei were labeled with 4′,6-diamidino-2-phenylindole (Molecular Probes, Invitrogen). Images were collected on a Zeiss epifluorescence microscope with AxioVision software.

Flow cytometry—Cells were harvested using Accutase (Sigma) and resuspended in FACS buffer (10% FBS, DMEM). After fixing in 2% PFA at RT for 30 minutes or stained alive, cells were incubated with primary antibody for 1 hr at RT, followed by incubation with appropriate secondary antibody for 1 hr at RT. Antibodies used are listed in the Key resources table.

Luciferase assays—To measure WNT pathway activity, WT and TKO cells were co-transfected with TCF/LEF luciferase reporter vector premixed with constitutively-expressing Renilla luciferase vector that serves as internal control for transfection efficiency (Promega) and lysed using the Dual-Glo Assay (Promega) after 24 hr. Luciferase assays were conducted according to the manufacturer's protocol (Promega). Luciferase signal was normalized to Renilla expression. All data were normalized to the signal obtained from WT hESCs. Assays were performed in duplicates and repeated at least three times.

Lentivirus infection—To generate inducible NKX2–5 and TET1 overexpression constructs, *NKX2–5* cDNA from day 6 WT CM differentiation and *TET1* cDNA from FH-TET1-pEF construct (Addgene 49792) were inserted into an all-in-one doxycycline-inducible lentiviral backbone with eGFP as selection marker (CS-TRE-PRE-Ubc-tTA-I2G) (Yamaguchi et al., 2012). To generate a lentiviral construct that contains gRNAs targeting the promoter of NKX2–5, we cloned three gRNAs and an mCherry selection marker into the pMuLE-Lenti-Dest-Neo backbone using Multiple Lentiviral Expression System Kit with gateway LR recombination. The MuLE system kit was a gift from Ian Frew (Addgene kit # 1000000060). The dCas9-TET1CD lentiviral construct was described previously

(Verma et al., 2018). The HEK293T cells were plated in a 10 cm dish and transfected with target plasmid and packaging plasmids using PEI. The transfected HEK293T cells were incubated for 2 days and medium was collected. Supernatant containing virus was concentrated by Lenti-X Concentrator according to the manufacturer's protocol (Clontech). hESCs were infected with lentivirus and isolated by FACS for GFP+ cells (NKX2–5 and TET1 overexpression) or GFP+/mCherry+ cells (dcas9-TET1+NKX2–5 promoter gRNAs). Sequences for gRNAs are in the Key resources table.

ChIP-qPCR—$0.5X10^6$ cells were used for each immunoprecipitation. ChIP was performed using the CUTANA ChIC / CUT&RUN Kit (Epicypher, 4–1048) according to the manufacturer's protocols. The antibodies and primers used for ChIP–qPCR are provided in Table S2.

PCR-based bisulfite sequencing—Bisulfite conversion was performed using the EZ DNA Methylation-Direct kit (Zymo Research). Converted DNA was amplified using Taq DNA Polymerase (NEB) and bisulfite-specific primer pairs (listed in Table S2). PCR amplicons were sent to Genewiz for next generation sequencing and aligned to target sequence to determine their methylation level.

RNA sequencing—For RNA sequencing, total RNA was isolated with the RNeasy Mini kit (QIAGEN, 74136) from WT and TKO HUES8 hESC-derived cells (n = 2 cultures each). RNA samples were submitted to WCMC Genomics Resources Core Facility for sequencing. RNA-seq data were aligned to the hg19 reference genome. RNA seq alignment, differential gene expression analysis and GSEA were performed as described (Anelli et al., 2017). Differentially expressed genes were defined by log2 fold change greater than 2 or less than −2 and an adjusted p value < 0.01.

ERRBS—For eRRBS (Enhanced Reduced Representation Bisulfite Sequencing), genomic DNA was isolated from WT or TKO HUES8 hESC-derived cells using DNeasy Blood & Tissue Kits (QIAGEN). Genomic DNA was submitted to the Weill Cornell Medicine Epigenomics core for eRRBS. The WCM Computational Genomics core facility supported alignment and methylation extraction for eRRBS data as described (Akalin et al., 2012). Briefly, DMRs were defined as regions containing at least five differentially methylated CpGs (DMCs; false discovery rate = 20%; chi-square test) and whole methylation was more than 10%. DMR calling was performed with RRBSeeqer with default parameters (Pan et al., 2015).

ChIP-seq and Analysis—ChIP-seq was performed as previously described (Dixon et al., 2021). Briefly, anti-V5 antibody (Cell Signaling Technology, D3H8Q) was used for immunoprecipitation. Libraries were prepared using the NEBNext® Ultra II DNA Library Prep Kit (NEB, E7103S) and NEBNext® Multiplex Oligos for Illumina® (Index Primers Set 1; NEB, E7335S). Samples were pooled and submitted to MSKCC Integrated Genomics Operation core for quality control and sequencing as follows. After PicoGreen quantification and quality control by Agilent BioAnalyzer, pooled libraries were run over one lane of a HiSeq 4000 in a 50bp/50bp paired end run, using the HiSeq 3000/4000 SBS Kit (Illumina). The loading concentration was 2nM and a 5% spike-in of PhiX was added to the run to

increase diversity and for quality control purposes. Sequencing data was aligned to the hg19 reference genome using mem module from bwa-0.7.17 (Li and Durbin, 2009). Peak calling was performed by macs14 1.4.2 with default parameters (Zhang et al., 2008).

Genomic Region Annotation—Genomic regions for CpGs were defined according to the following definitions. Promoters were defined as the regions encompassing 1 kb upstream and downstream of the TSS of RefSeq genes. The following characteristics were used to classify promoters as active, initiated, bivalent and silent. Active promoters were associated with H3K4me3 but not H3K27me3 (in the 2kb region flanking the TSS). Bivalent promoters were associated with H3K4me3 and H3K27me3 (in the 2kb region flanking the TSS). Silent promoters were not associated with H3K4me3 (in the 2kb region flanking the TSS). Enhancers were defined as regions outside of promoters and exons. Poised enhancers were identified as regions overlapping H3K4me1 peaks only. Active enhancers were identified as regions overlapping H3K4me1 and H3K27ac peaks. Overlap of 5mC changes with histone marks was determined using previous ChIP–seq datasets for histone marks (Zhang et al., 2019)

Genomic Regions Enrichment of Annotations Tool (GREAT)—GREAT Analysis was performed using the GREAT tool (McLean et al., 2010). The following parameters were used: DMRs in promoter: 2 kb upstream and 2 kb downstream around TSS. DMRs in enhancer: DMRs overlapped with enhancer marks H3K4me1 and/or H3K27ac and associated with single nearest gene.

Motif analysis—Analysis of motif enrichment (AME) was performed using MEME Suite 5.5.5 with default parameters (McLeay and Bailey, 2010).

QUANTIFICATION AND STATISTICAL ANALYSIS

Statistical analyses were implemented with Prism 7. Data are presented as means ± sem (unless otherwise noted) and were derived from at least three independent experiments. Statistical analysis was performed using two-tailed Student’s t test. The distribution of the raw data approximated a normal distribution (Kolmogorov–Smirnov normality test) for data with a sufficient number of replicates to test for normality. statistical details of experiments can be found in the figure legends.

Supplementary Material

Refer to Web version on PubMed Central for supplementary material.

ACKNOWLEDGMENTS

The authors thank the WCM Flow Cytometry Core for cell sorting, the WCM Epigenomics Core, Genomics Resources Core, and MSKCC Integrated Genomics Operation core for performing eRRBS, RNA sequencing, and CHIP-seq, respectively. These studies were supported by a grant (2016–032) from the Tri-Institutional Stem Cell Initiative (T.E. and D.H).

REFERENCES

Akalin A, Garrett-Bakelman FE, Kormaksson M, Busuttil J, Zhang L, Khrebtukova I, Milne TA, Huang Y, Biswas D, Hess JL, et al. (2012). Base-pair resolution DNA methylation sequencing reveals profoundly divergent epigenetic landscapes in acute myeloid leukemia. PLoS Genet. 8, e1002781. [PubMed: 22737091]

Almeida RD, Loose M, Sottile V, Matsa E, Denning C, Young L, Johnson AD, Gering M, and Ruzov A (2012). 5-hydroxymethyl-cytosine enrichment of non-committed cells is not a universal feature of vertebrate development. Epigenetics 7, 383–389. [PubMed: 22419071]

Anelli V, Villefranc JA, Chhangawala S, Martinez-McFaline R, Riva E, Nguyen A, Verma A, Bareja R, Chen Z, Scognamiglio T, et al. (2017). Oncogenic BRAF disrupts thyroid morphogenesis and function via twist expression. eLife 6, e20728. [PubMed: 28350298]

Burridge PW, Sharma A, and Wu JC (2015). Genetic and epigenetic regulation of human cardiac reprogramming and differentiation in regenerative medicine. Annu. Rev. Genet. 49, 461–484. [PubMed: 26631515]

Dai HQ, Wang BA, Yang L, Chen JJ, Zhu GC, Sun ML, Ge H, Wang R, Chapman DL, Tang F, et al. (2016). TET-mediated DNA demethylation controls gastrulation by regulating Lefty-Nodal signalling. Nature 538, 528–532. [PubMed: 27760115]

Dawlaty MM, Breiling A, Le T, Barrasa MI, Raddatz G, Gao Q, Powell BE, Cheng AW, Faull KF, Lyko F, and Jaenisch R (2014). Loss of Tet enzymes compromises proper differentiation of embryonic stem cells. Dev. Cell 29, 102–111. [PubMed: 24735881]

Dixon G, Pan H, Yang D, Rosen BP, Jashari T, Verma N, Pulecio J, Caspi I, Lee K, Stransky S, et al. (2021). QSER1 protects DNA methylation valleys from de novo methylation. Science 372, eabd0875. [PubMed: 33833093]

Evans SM, Yelon D, Conlon FL, and Kirby ML (2010). Myocardial lineage development. Circ. Res. 107, 1428–1444. [PubMed: 21148449]

Fan J, Zhang Y, Mu J, He X, Shao B, Zhou D, Peng W, Tang J, Jiang Y, Ren G, and Xiang T (2018). TET1 exerts its anti-tumor functions via demethylating DACT2 and SFRP2 to antagonize Wnt/β-catenin signaling pathway in nasopharyngeal carcinoma cells. Clin. Epigenetics 10, 103. [PubMed: 30075814]

Fang S, Li J, Xiao Y, Lee M, Guo L, Han W, Li T, Hill MC, Hong T, Mo W, et al. (2019). Tet inactivation disrupts YY1 binding and long-range chromatin interactions during embryonic heart development. Nat. Commun. 10, 4297. [PubMed: 31541101]

Friedman CE, Nguyen Q, Lukowski SW, Helfer A, Chiu HS, Miklas J, Levy S, Suo S, Han JJ, Osteil P, et al. (2018). Single-cell transcriptomic analysis of cardiac differentiation from human PSCs reveals HOPX-dependent cardiomyocyte maturation. Cell Stem Cell 23, 586–598.e8. [PubMed: 30290179]

Gilsbach R, Preissl S, Grüning BA, Schnick T, Burger L, Benes V, Würch A, Bönisch U, Günther S, Backofen R, et al. (2014). Dynamic DNA methylation orchestrates cardiomyocyte development, maturation and disease. Nat. Commun. 5, 5288. [PubMed: 25335909]

Gilsbach R, Schwaderer M, Preissl S, Grüning BA, Kranzhöfer D, Schneider P, Nührenberg TG, Mulero-Navarro S, Weichenhan D, Braun C, et al. (2018). Distinct epigenetic programs regulate cardiac myocyte development and disease in the human heart in vivo. Nat. Commun. 9, 391. [PubMed: 29374152]

Greco CM, Kunderfranco P, Rubino M, Larcher V, Carullo P, Anselmo A, Kurz K, Carell T, Angius A, Latronico MV, et al. (2016). DNA hydroxymethylation controls cardiomyocyte gene expression in development and hypertrophy. Nat. Commun. 7, 12418. [PubMed: 27489048]

Homsy J, Zaidi S, Shen Y, Ware JS, Samocha KE, Karczewski KJ, DePalma SR, McKean D, Wakimoto H, Gorham J, et al. (2015). De novo mutations in congenital heart disease with neurodevelopmental and other congenital anomalies. Science 350, 1262–1266. [PubMed: 26785492]

Khoueiry R, Sohni A, Thienpont B, Luo X, Velde JV, Bartoccetti M, Boeckx B, Zwijsen A, Rao A, Lambrechts D, and Koh KP (2017). Lineage-specific functions of TET1 in the postimplantation mouse embryo. Nat. Genet. 49, 1061–1072. [PubMed: 28504700]

Koh KP, Yabuuchi A, Rao S, Huang Y, Cunniff K, Nardone J, Laiho A, Tahiliani M, Sommer CA, Mostoslavsky G, et al. (2011). Tet1 and Tet2 regulate 5-hydroxymethylcytosine production and cell lineage specification in mouse embryonic stem cells. Cell Stem Cell 8, 200–213. [PubMed: 21295276]

Kohli RM, and Zhang Y (2013). TET enzymes, TDG and the dynamics of DNA demethylation. Nature 502, 472–479. [PubMed: 24153300]

Kunimoto H, Fukuchi Y, Sakurai M, Sadahira K, Ikeda Y, Okamoto S, and Nakajima H (2012). Tet2 disruption leads to enhanced self-renewal and altered differentiation of fetal liver hematopoietic stem cells. Sci. Rep. 2, 273. [PubMed: 22355785]

Lan Y, Pan H, Li C, Banks KM, Sam J, Ding B, Elemento O, Goll MG, and Evans T (2019). TETs regulate proepicardial cell migration through extracellular matrix organization during zebrafish cardiogenesis. Cell Rep. 26, 720–732.e4. [PubMed: 30650362]

Langlois T, da Costa Reis Monte-Mor B, Lenglet G, Droin N, Marty C, Le Couédic JP, Almire C, Auger N, Mercher T, Delhommeau F, et al. (2014). TET2 deficiency inhibits mesoderm and hematopoietic differentiation in human embryonic stem cells. Stem Cells 32, 2084–2097. [PubMed: 24723429]

Lee H, and Evans T (2019). TMEM88 inhibits Wnt signaling by promoting Wnt signalosome localization to multivesicular bodies. iScience 19, 267–280. [PubMed: 31401350]

Lee J, Shao NY, Paik DT, Wu H, Guo H, Termglinchan V, Churko JM, Kim Y, Kitani T, Zhao MT, et al. (2018). SETD7 drives cardiac lineage commitment through stage-specific transcriptional activation. Cell Stem Cell 22, 428–444.e5. [PubMed: 29499155]

Li H, and Durbin R (2009). Fast and accurate short read alignment with Burrows-Wheeler transform. Bioinformatics 25, 1754–1760. [PubMed: 19451168]

Li C, Lan Y, Schwartz-Orbach L, Korol E, Tahiliani M, Evans T, and Goll MG (2015a). Overlapping requirements for Tet2 and Tet3 in normal development and hematopoietic stem cell emergence. Cell Rep. 12, 1133–1143. [PubMed: 26257178]

Li T, Yang D, Li J, Tang Y, Yang J, and Le W (2015b). Critical role of Tet3 in neural progenitor cell maintenance and terminal differentiation. Mol. Neurobiol. 51, 142–154. [PubMed: 24838624]

Li X, Yue X, Pastor WA, Lin L, Georges R, Chavez L, Evans SM, and Rao A (2016). Tet proteins influence the balance between neuroectodermal and mesodermal fate choice by inhibiting Wnt signaling. Proc. Natl. Acad. Sci. USA 113, E8267–E8276. [PubMed: 27930333]

Li J, Wu X, Zhou Y, Lee M, Guo L, Han W, Mo W, Cao WM, Sun D, Xie R, and Huang Y (2018). Decoding the dynamic DNA methylation and hydroxymethylation landscapes in endodermal lineage intermediates during pancreatic differentiation of hESC. Nucleic Acids Res. 46, 2883–2900. [PubMed: 29394393]

Lian X, Hsiao C, Wilson G, Zhu K, Hazeltine LB, Azarin SM, Raval KK, Zhang J, Kamp TJ, and Palecek SP (2012). Robust cardiomyocyte differentiation from human pluripotent stem cells via temporal modulation of canonical Wnt signaling. Proc. Natl. Acad. Sci. USA 109, E1848–E1857. [PubMed: 22645348]

Ma R, Feng N, Yu X, Lin H, Zhang X, Shi O, Zhang H, Zhang S, Li L, Zheng M, et al. (2017). Promoter methylation of Wnt/β-Catenin signal inhibitor *TMEM88* is associated with unfavorable prognosis of non-small cell lung cancer. Cancer Biol. Med. 14, 377–386. [PubMed: 29372104]

McLean CY, Bristor D, Hiller M, Clarke SL, Schaar BT, Lowe CB, Wenger AM, and Bejerano G (2010). GREAT improves functional interpretation of cis-regulatory regions. Nat. Biotechnol. 28, 495–501. [PubMed: 20436461]

McLeay RC, and Bailey TL (2010). Motif enrichment analysis: A unified framework and an evaluation on ChIP data. BMC Bioinformatics 11, 165. [PubMed: 20356413]

Moran-Crusio K, Reavie L, Shih A, Abdel-Wahab O, Ndiaye-Lobry D, Lobry C, Figueroa ME, Vasanthakumar A, Patel J, Zhao X, et al. (2011). Tet2 loss leads to increased hematopoietic stem cell self-renewal and myeloid transformation. Cancer Cell 20, 11–24. [PubMed: 21723200]

Murry CE, and Keller G (2008). Differentiation of embryonic stem cells to clinically relevant populations: lessons from embryonic development. Cell 132, 661–680. [PubMed: 18295582]

Nimura K, Ura K, Shiratori H, Ikawa M, Okabe M, Schwartz RJ, and Kaneda Y (2009). A histone H3 lysine 36 trimethyltransferase links Nkx2–5 to Wolf-Hirschhorn syndrome. Nature 460, 287–291. [PubMed: 19483677]

Novikov N, and Evans T (2013). Tmem88a mediates GATA-dependent specification of cardiomyocyte progenitors by restricting WNT signaling. Development 140, 3787–3798. [PubMed: 23903195]

Palpant NJ, Pabon L, Rabinowitz JS, Hadland BK, Stoick-Cooper CL, Paige SL, Bernstein ID, Moon RT, and Murry CE (2013). Transmembrane protein 88: a Wnt regulatory protein that specifies cardiomyocyte development. Development 140, 3799–3808. [PubMed: 23924634]

Pan H, Jiang Y, Boi M, Tabbò F, Redmond D, Nie K, Ladetto M, Chiappella A, Cerchietti L, Shaknovich R, et al. (2015). Epigenomic evolution in diffuse large B-cell lymphomas. Nat. Commun. 6, 6921. [PubMed: 25891015]

Verma N, Pan H, Doré LC, Shukla A, Li QV, Pelham-Webb B, Teijeiro V, González F, Krivtsov A, Chang CJ, et al. (2018). TET proteins safeguard bivalent promoters from de novo methylation in human embryonic stem cells. Nat. Genet. 50, 83–95. [PubMed: 29203910]

Wu X, and Zhang Y (2017). TET-mediated active DNA demethylation: mechanism, function and beyond. Nat. Rev. Genet. 18, 517–534. [PubMed: 28555658]

Wu H, D'Alessio AC, Ito S, Xia K, Wang Z, Cui K, Zhao K, Sun YE, and Zhang Y (2011). Dual functions of Tet1 in transcriptional regulation in mouse embryonic stem cells. Nature 473, 389–393. [PubMed: 21451524]

Yamaguchi T, Hamanaka S, Kamiya A, Okabe M, Kawarai M, Wakiyama Y, Umino A, Hayama T, Sato H, Lee YS, et al. (2012). Development of an all-in-one inducible lentiviral vector for gene specific analysis of reprogramming. PLoS ONE 7, e41007. [PubMed: 22815895]

Zadeh FJ, Akbari T, Zayeri ZD, Samimi A, Davari N, and Rezaeeyan H (2020). The role of molecular mechanism of ten-eleven translocation2 (TET2) family proteins in pathogenesis of cardiovascular diseases (CVDs). Mol. Biol. Rep. 47, 5503–5509. [PubMed: 32572734]

Zhang Y, Liu T, Meyer CA, Eeckhoute J, Johnson DS, Bernstein BE, Nusbaum C, Myers RM, Brown M, Li W, and Liu XS (2008). Model-based analysis of ChIP-seq (MACS). Genome Biol. 9, R137. [PubMed: 18798982]

Zhang Y, Li T, Preissl S, Amaral ML, Grinstein JD, Farah EN, Destici E, Qiu Y, Hu R, Lee AY, et al. (2019). Transcriptionally active HERV-H retrotransposons demarcate topologically associating domains in human pluripotent stem cells. Nat. Genet. 51, 1380–1388. [PubMed: 31427791]

Highlights

- Human cardiomyocyte differentiation is coupled to DNA methylation changes
- Loss of TET enzymes impairs human cardiomyocyte differentiation
- Mutant cells have defects in mesoderm patterning and progenitor specification
- TETs regulate the methylation and expression of *TMEM88* and *NKX2–5*

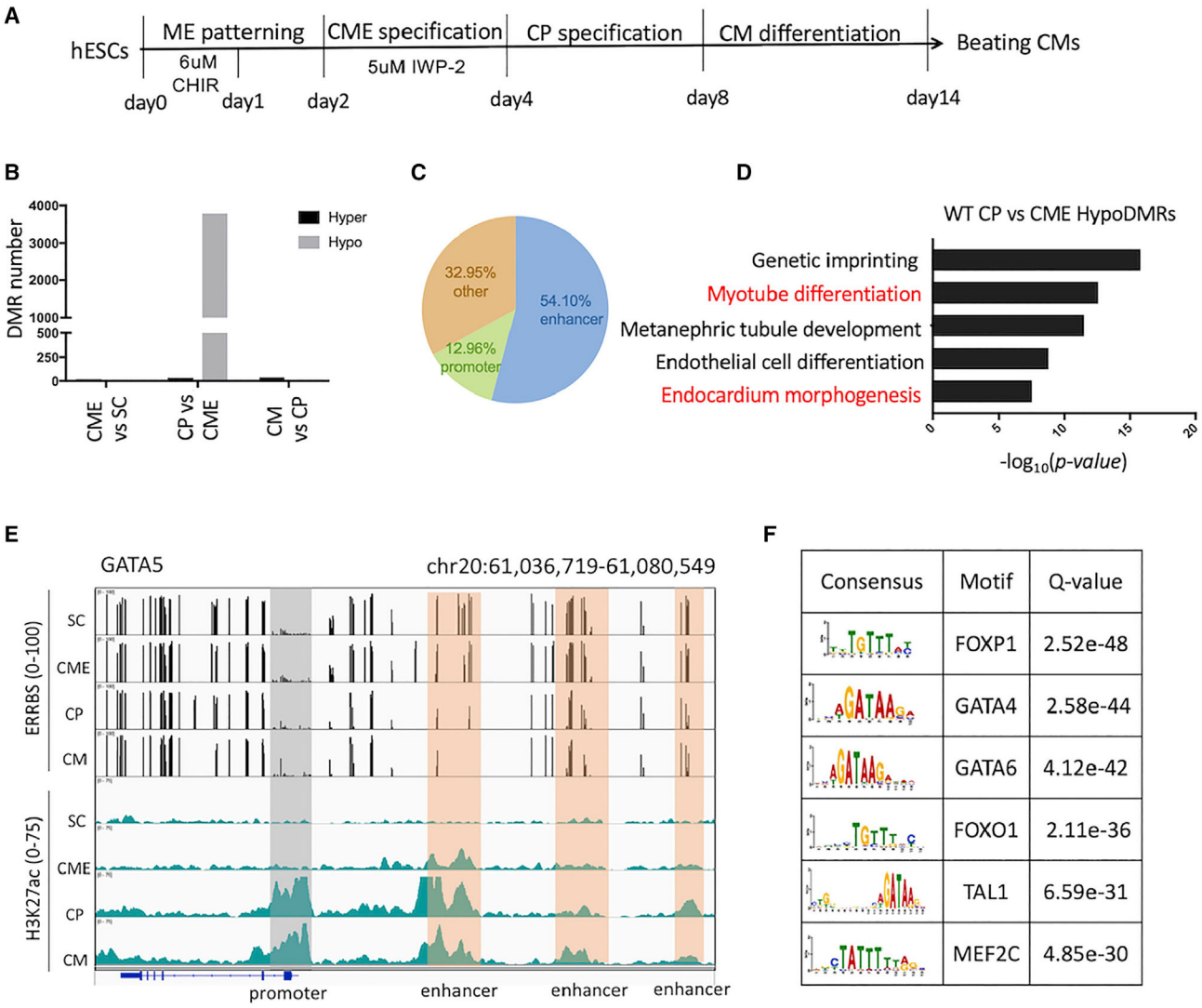

Figure 1. DNA methylation dynamics during cardiomyocyte differentiation

(A) Scheme of cardiomyocyte differentiation protocol indicating the timing and use of different small molecules. CHIR, GSK3 inhibitor to activate WNT pathway; IWP2, WNT pathway inhibitor; ME, mesoderm; CME, cardiac mesoderm; CP, cardiac progenitor; CM, cardiomyocyte.

(B) Numbers of DMRs that show increased (hyper-DMR) or reduced (hypo-DMR) DNA methylation through each CM differentiation stage transition.

(C) Enrichment of various regulatory regions associated with WT CP-CME hypo-DMRs. Total DMR number = 3,786.

(D) GREAT analysis of WT CP-CME hypo-DMRs shows they are enriched for cardiac development genes.

(E) Representative genome browser view illustrating the DNA methylation and H3K27ac dynamics at genomic regions surrounding *GATA5* during CM differentiation. Gray box indicates promoter region with DNA demethylation. Orange boxes indicate enhancer regions

with DNA demethylation. Promoter and enhancer annotation is based on genomic position and active histone mark H3K27ac. H3K27ac dataset is from GEO: GSE116862.
(F) Consensus motif analysis in WT CP-CME hypo-DMRs indicates the enrichment of motifs for transcription factors important for cardiac specification.
See also Figure S1.

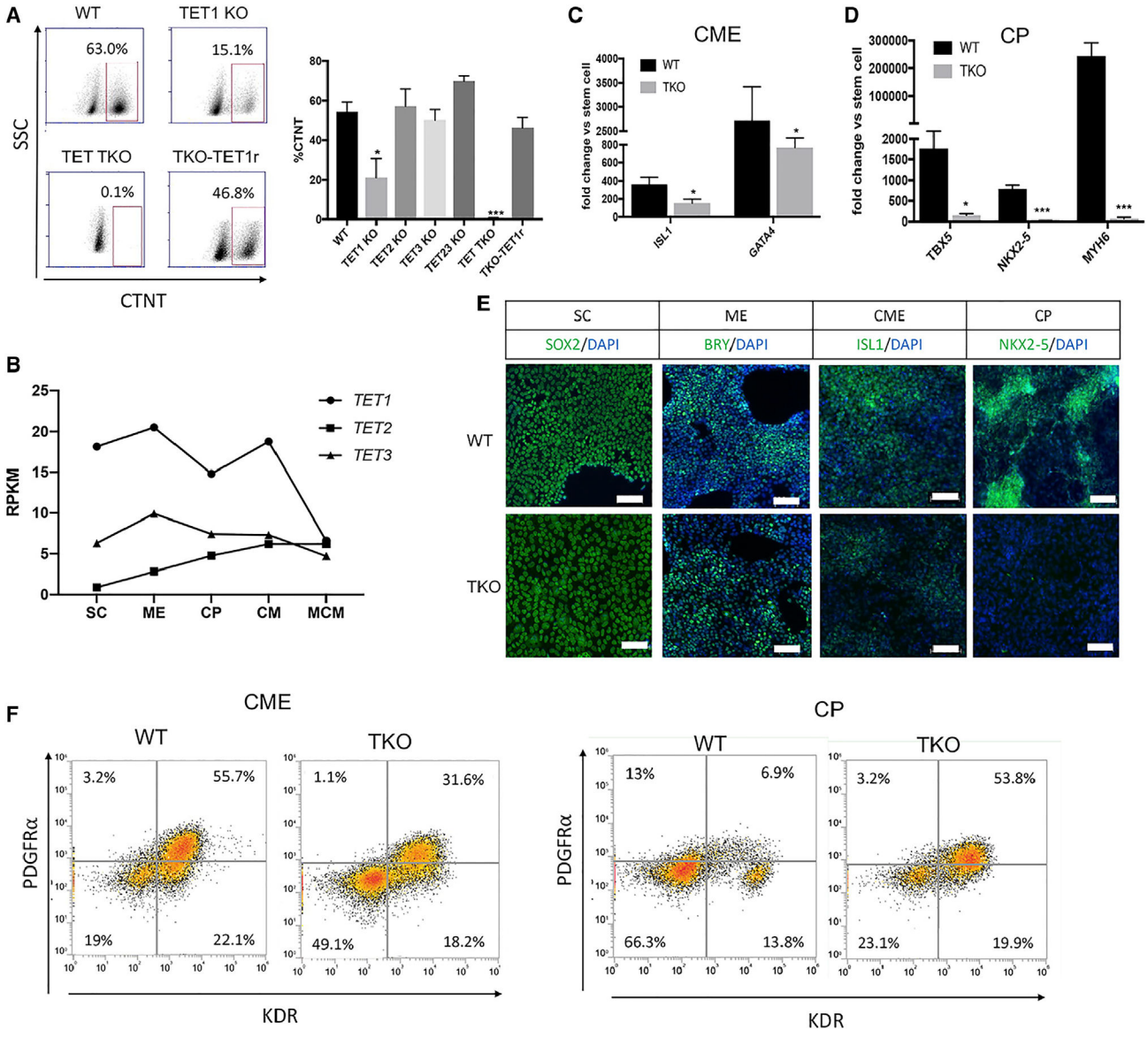

Figure 2. TET TKO hESCs exhibit cardiomyocyte differentiation defects

(A) Flow cytometry for quantitative analysis of CTNT^{+} cells at day 14 (no lactate treatment). Shown are representative plots, whereas the bar graphs represent at least three independent differentiation experiments. TET TKO, TET1/2/3 triple knockout; TKO-TET1r, repair of one *TET1* mutant allele to the WT sequence in TKO hESCs by CRISPR-Cas9-directed homology-mediated repair.

(B) Expression levels of *TET1*, *TET2*, and *TET3* based on RNA-seq during CM differentiation. SC, stem cell; MCM, mature cardiomyocyte (day 30). Dataset from GEO: GSE116862.

(C) qPCR analysis of cardiac mesoderm markers *ISL1* and *GATA4* in WT and TET TKO derived cells at day 3.

(D) qPCR analysis of cardiac progenitor markers *TBX5*, *NKX2–5*, and *MYH6* in WT and TET-TKO-derived cells at day 6.

(E) Time course immunofluorescence analysis of stage-specific markers during WT and TET TKO cardiac differentiation. White scale bars are 100 μM.
(F) Representative flow cytometry of PDGFRα$^+$ and KDR$^+$ cells with day 3 (CME stage) or day 6 (CP stage) WT and TKO cells.
Significance is indicated as *$p < 0.05$, ***$p < 0.001$, ns indicates not significant. Data are presented as means ± SEM derived from at least three independent biological replicates. See also Figure S2.

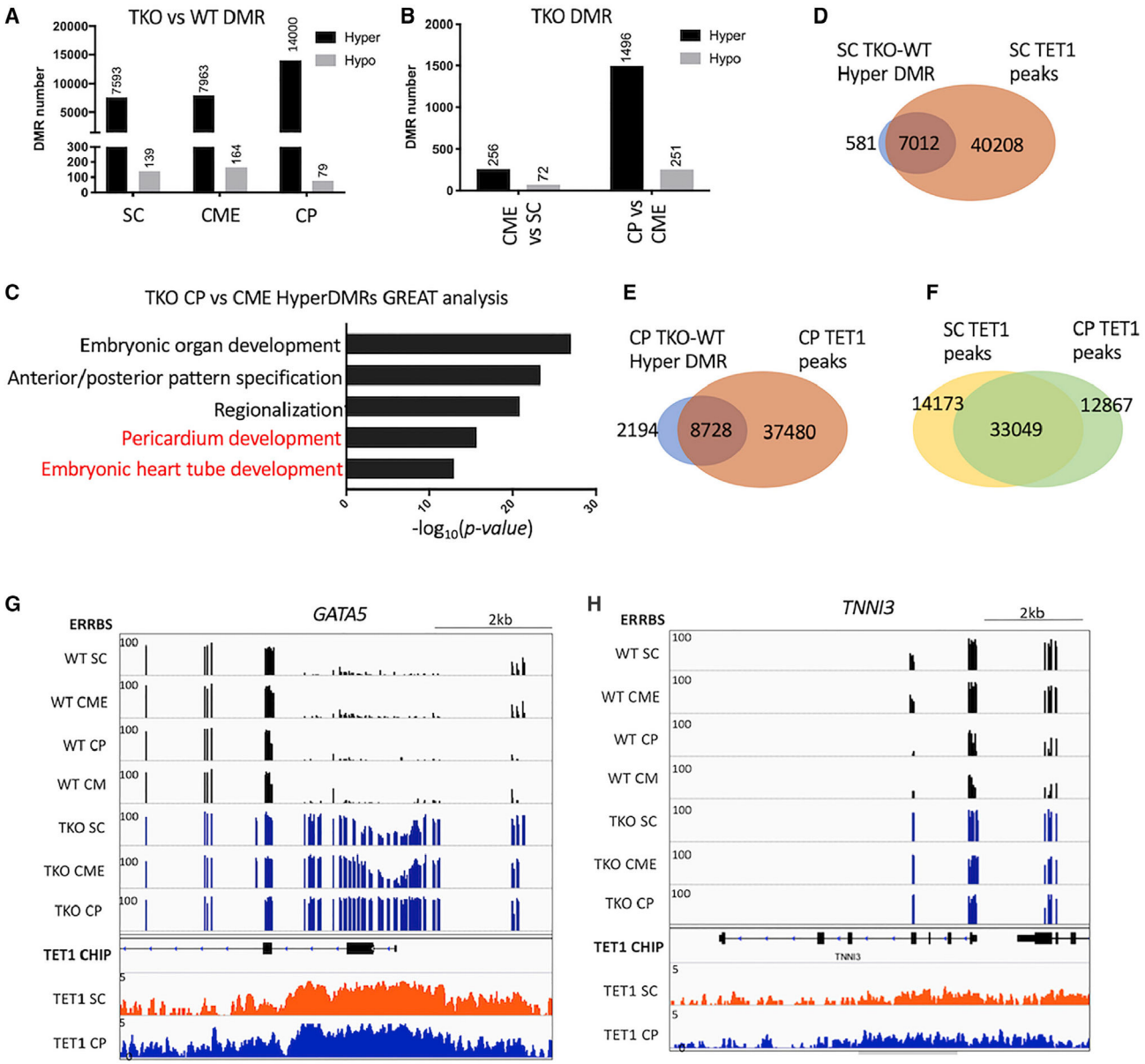

Figure 3. Dynamic regulation of methylation through TET enzymes during CM differentiation

(A) Numbers of differentially methylated regions (DMRs) that show increased (hyper-DMR) or reduced (hypo-DMR) DNA methylation for TKO cells as compared with WT cells at each differentiation stage.

(B) Numbers of DMRs that show increased (hyper-DMR) or reduced (hypo-DMR) DNA methylation when WT and TKO cells progress through to the CP specification stage.

(C) GREAT analysis of TKO CP-CME hyper-DMRs shows they are enriched for cardiac development genes.

(D and E) Venn diagrams indicate most TKO-WT hyper-DMRs identified at SC or CP stages overlap with TET1 binding peaks found in WT cells.

(F) Venn diagram indicates the number of overlapping or distinct TET1 binding peaks identified at the SC and CP stages in WT cells.

(G and H) Representative genome browser views illustrating the DNA methylation dynamics and TET1 binding at genomic regions surrounding *GATA5* and *TNNI3* during CM differentiation.

See also Figure S3.

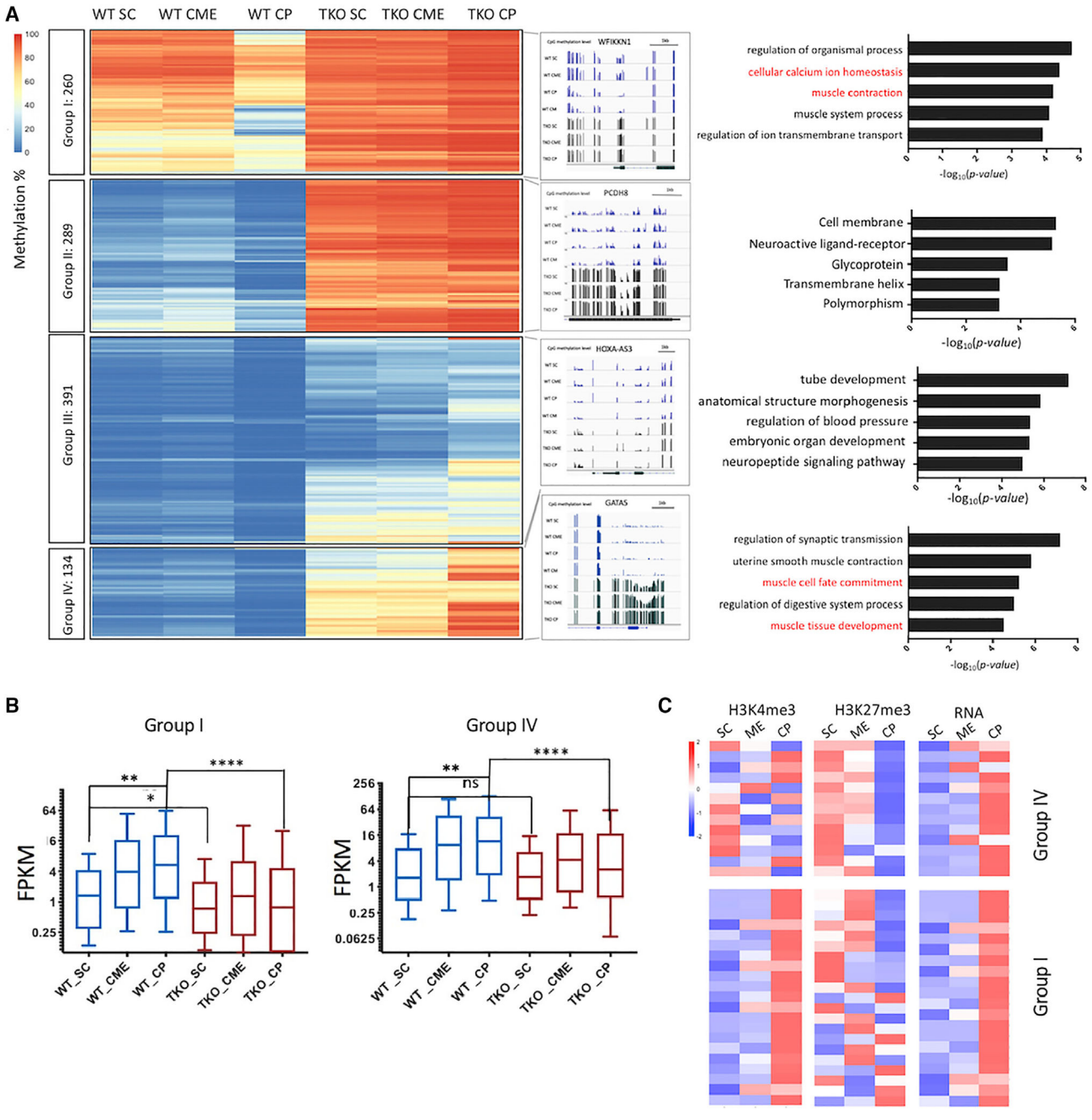

Figure 4. Distinct promoter methylation signatures for different categories of genes

(A) Left panel: heatmaps showing the average levels of DNA methylation for promoters (1 kb upstream and downstream of the transcription start site) that have methylation differences between WT and TKO cells or show dynamic methylation changes during differentiation. Middle panel: examples of each group showing methylation level by eRRBS. Right panel: GO analysis showing biological process enriched in each group.

(B) Boxplots showing the transcript expression levels of genes in group I and group IV during CP specification based on RNA-seq profiles.

(C) Heatmaps showing the average levels of H3K4me3, H3K27me3, and RNA for promoters of cardiac regulatory genes in group IV and cardiac contraction genes in group I.
See also Figure S4 and Table S1.

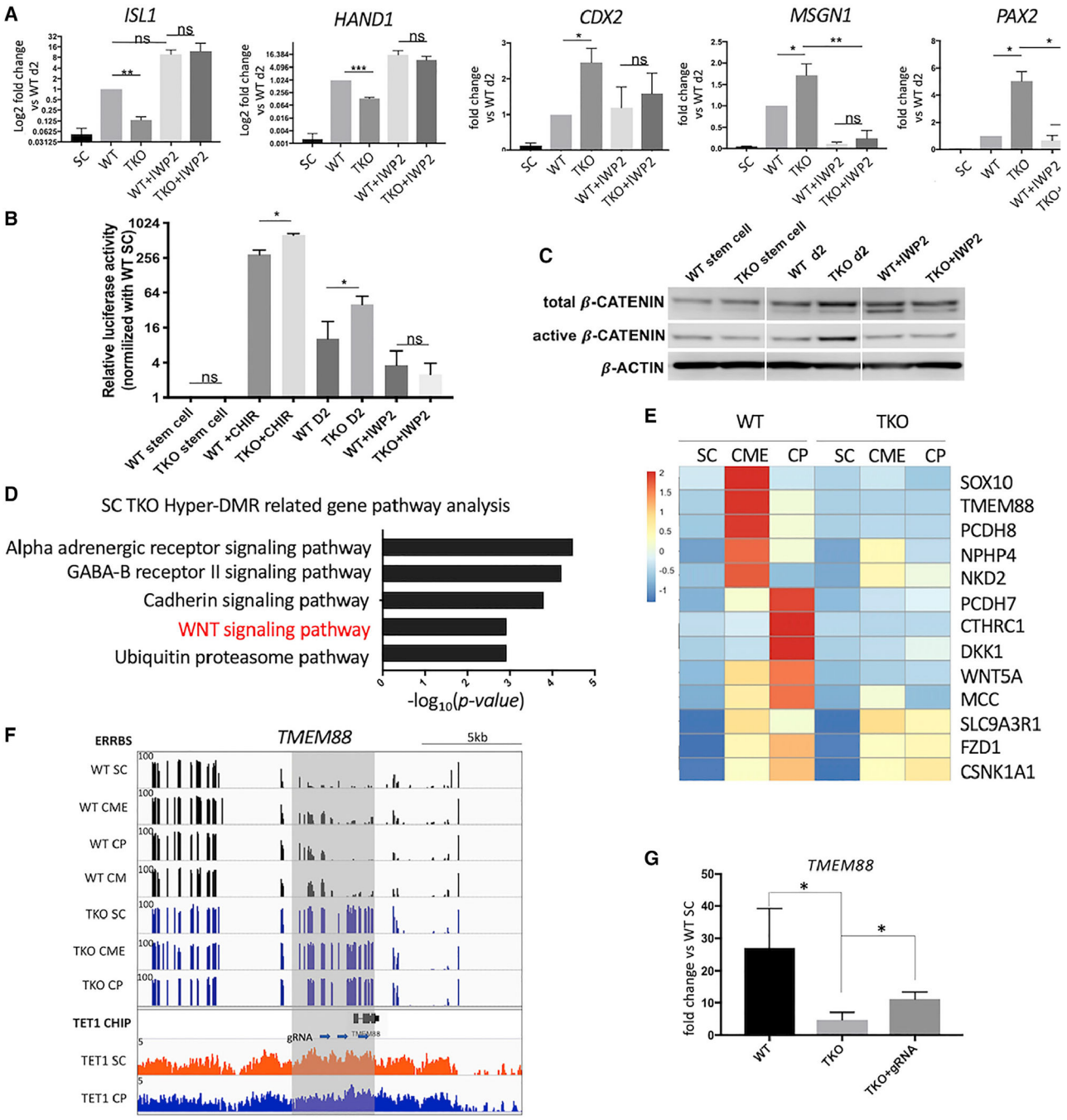

Figure 5. TETs influence mesoderm patterning by regulating the expression and DNA modification status of genes encoding WNT inhibitors

(A) qPCR analysis of LM markers *ISL1* and *HAND1*, PM markers *CDX2* and *MSGN1*, and IM marker *PAX2* at day 2 of differentiation, with or without IWP2 treatment from day 1 to day 2.

(B) TopFlash luciferase reporter activity, normalized to *Renilla* luciferase levels in stem cells, for day 1 cells after CHIR treatment and day 2 cells with or without IWP2 treatment.

(C) Representative western blots analyzing total or active β-catenin under the indicated conditions.

(D) Pathway analysis for promoter hyper-DMR associated genes in TKO cells at the SC stage.

E) Relative gene expression levels of WNT inhibitory genes that in TKO cells show promoter hyper-DMR during WT or TKO differentiation based on RNA-seq profiles.

(F) Representative genome browser view illustrating the DNA methylation dynamics and TET1 binding at genomic regions surrounding the *TMEM88* promoter during CM differentiation. Blue arrows: gRNAs used to recruit dCas9-TET1 to the *TMEM88* promoter and induce locus specific demethylation.

(G) qPCR analysis of relative *TMEM88* expression levels at day 2 of CM differentiation for WT or TKO ESCs compared with those TKO cells expressing dCas9-TET1 fusion protein and *TMEM88*-targeting gRNAs.

Significance is indicated as *$p < 0.05$, **$p < 0.01$, ns indicates not significant. Data are presented as means ± SEM derived from at least three independent biological replicates. See also Figures S5 and S6.

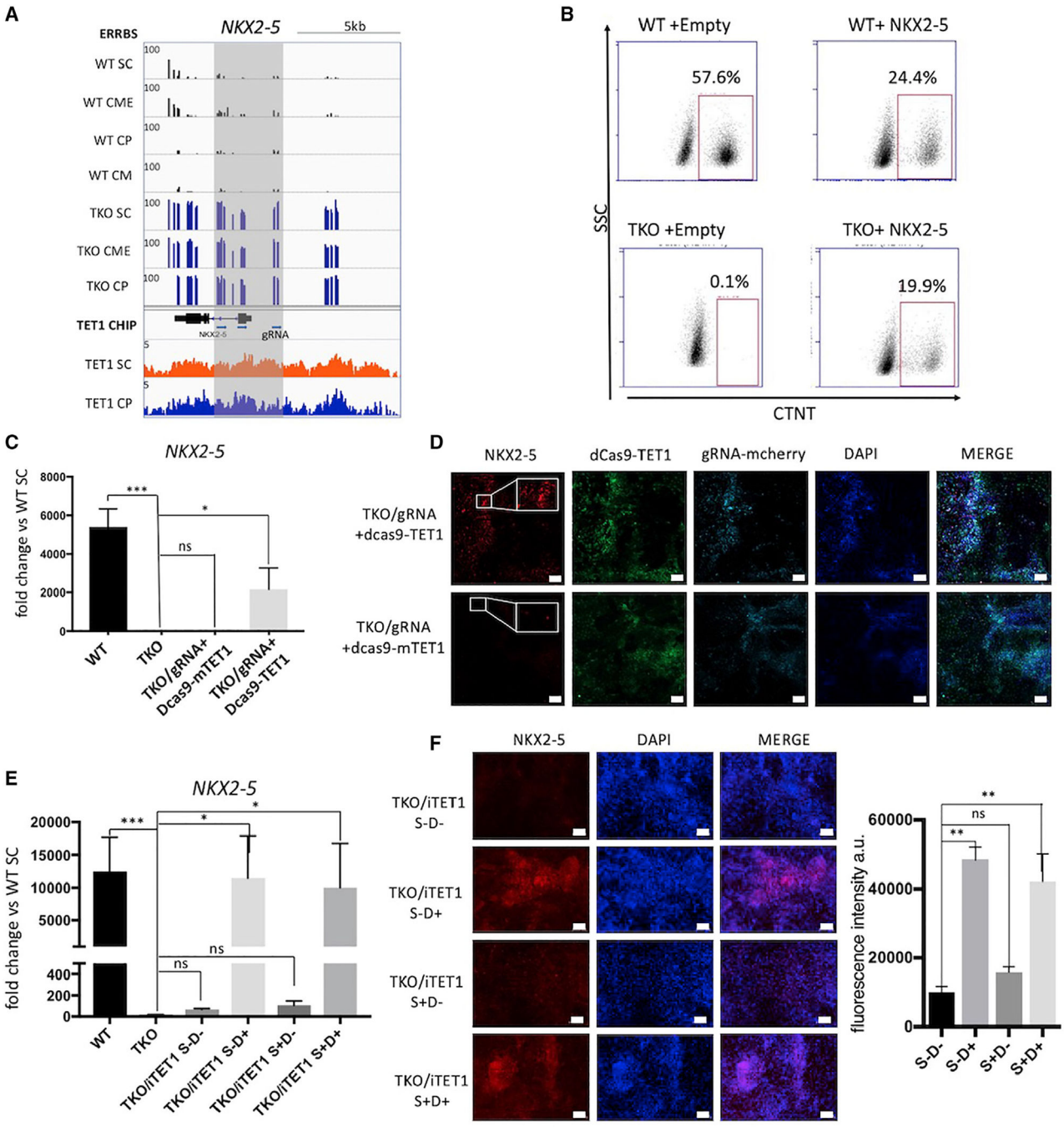

Figure 6. TETs directly regulate *NKX2–5* through modifying methylation status of the *NKX2–5* promoter

(A) Representative genome browser view illustrating the DNA methylation dynamics and TET1 binding at genomic regions surrounding the *NKX2*-5 promoter during CM differentiation. Blue arrows: gRNAs used to recruit dCas9-TET1 to the *NKX2–5* promoter and induce locus specific demethylation.

(B) Flow cytometry of $CTNT^{+}$ cells at day 14 with doxycycline treatment from day 4 to day 6 in WT and TKO cells infected with a vector for doxycycline-induced *NKX2–5* expression or empty vector.

(C) qPCR analysis of *NKX2–5* expression on day 8 of CM differentiation for TKO ESCs expressing NKX2–5-targeting gRNAs with dCas9-mutTET1 or dCas9-TET1 fusion protein.
(D) Immunofluorescence of NKX2–5, EGFP (representing dCas9-TET1 or dCas9-mutTET1 expression), mCherry (representing gRNAs expression), and DAPI on day 8 of CM differentiation for TKO ESCs infected with gRNAs and dCas9-TET1 (NKX2–5 fluorescence intensity = 17,189 ± 2697 a.u.) or mutTET1 fusion protein (NKX2–5 fluorescence intensity = 1,585 ± 668 a.u.). Insert box shows magnified view. White scale bars are 100 μM.
(E) qPCR analysis of *NKX2–5* expression on day 8 of CM differentiation for TKO ESCs expressing doxycycline-induced TET1 protein in different time windows. S, stem cell stage; D, differentiation stage.
(F) Right panel: immunofluorescence of NKX2–5 on day 8 of CM differentiation for TKO ESCs expressing doxycycline-induced TET1 protein in different time windows. Left panel: mean fluorescence intensity of NKX2–5 expression on day 8 of CM differentiation for TKO ESCs expressing doxycycline-induced TET1 protein in different time window. White scale bars are 100 μM.
Significance is indicated as *$p < 0.05$, **$p < 0.01$, ***$p < 0.001$, ns indicates not significant. Data are presented as means ± SEM derived from at least three independent biological replicates. See also Figure S7.

Table 1.

Transcript levels of 21 WNT inhibitory genes with hyper-methylated promoters in WT and TKO differentiation

Gene	WT_SC (FPKM)	WT_CME (FPKM)	WT_CP (FPKM)	TKO_SC (FPKM)	TKO_CME (FPKM)	TKO_CP (FPKM)
WNT5A	3.243	479.896	672.983	10.657	60.375	85.911
PCDH7	4.675	262.028	671.323	16.109	116.678	158.288
FZD1	1.647	37.625	51.102	4.303	34.179	37.018
SOX10	2.542	20.755	2.297	0.745	2.13	0
CTHRC1	3.151	8.669	83.465	1.248	0.704	1.455
EGR1	60.03	27.02	20.932	38.638	21.002	41.987
DDIT3	0.886	9.834	12.964	2.011	17.406	31.061
DKK1	0.079	2.251	32.538	0.33	1.752	6.028
NPHP4	5.873	106.815	47.31	7.44	59.629	25.656
TMEM88	0.117	524.033	139.125	0.272	4.969	3.095
AMER2	0.561	2.11	12.323	0.855	20.577	39.467
SHISA6	0.82	19.297	7.836	1.162	27.129	1.224
PCDH8	0.524	13.758	4.341	0.766	1.338	1.062
MCC	13.391	201.004	323.845	16.881	141.113	31.316
NKD2	4.221	12.008	4.171	3.646	7.987	6.559
CSNK1A1	84.501	402.281	576.899	81.153	411.919	492.245
SLC9A3R1	41.31	297.429	210.741	40.066	299.385	248.793
SIAH2	13.211	55.832	42.027	12.82	63.503	166.853
NOTUM	1.306	16.369	3.069	1.15	35.828	0.67
TLE1	47.892	36.211	84.737	48.559	122.654	151.352
MESP1	0.192	5.261	2.05	0.19	9.855	0.231

KEY RESOURCES TABLE

REAGENT or RESOURCE	SOURCE	IDENTIFIER
Antibodies		
SOX2	Invitrogen	RRID:AB_2533841
BRY	R&D	RRID:AB_2303014
ISL1	abcam	RRID:AB_10703990
NKX2–5	Santa Cruz Biotechnology	RRID:AB_11149571
PAX2	R&D	RRID:AB_10889828
total beta-CATENIN	Cell Signaling	9562
active beta-CATENIN	Cell Signaling	8814s
beta-ACTIN	Sigma	RRID:AB_476692
CTNT	Abcam	RRID:AB_2206574
PDGFRa-APC	R&D	fab1264a
KDR-PE	R&D	RRID:AB_357165
BRY-PE	R&D	RRID:AB_2271455
SOX17	R&D	RRID:AB_355060
KRT7	Abcam	ab119697
TET1	Genetex	RRID:AB_11172316
V5-tag	cell signaling	RRID:AB_2687461
Bacterial and virus strains		
One Shot TOP10 Chemically Competent *E. coli*	Invitrogen	C404010
Chemicals, peptides, and recombinant proteins		
CHIR99021	Sigma-Aldrich	SML1046
IWP2	Sigma-Aldrich	I0536
B27	GIBCO	17504044
B-27 Supplement, minus insulin	GIBCO	A1895601
L-lactate	Sigma-Aldrich	L7022
human recombinant ACTIVIN A	R&D Systems	338-AC
Protease/Phosphatase inhibitor	Cell Signaling	5872
Critical commercial assays		
RNeasy Mini kit	QIAGEN	74106
Superscript III First-Strand Synthesis System	Invitrogen	18080051
LightCycler 480 Sybr Green master mix	Roche	04–887-352–001
CUTANA ChIC / CUT&RUN Kit	Epicypher	4–1048
EZ DNA Methylation-Direct kit	Zymo Research	D5021
DNeasy Blood & Tissue Kits	QIAGEN	69506
NEBNext Ultra II DNA Library Prep Kit	NEB	E7103S
Dual-Glo Luciferase Assay System	Promega	E2920

REAGENT or RESOURCE	SOURCE	IDENTIFIER
Multiple Lentiviral Expression System Kit	Addgene	kit # 1000000060
Deposited data		
Raw and analyzed data	This paper	GSE186848
Histone datasets	Zhang et al., 2019	GSE116862
WT and TKO stem cell RNA seq data	Verma et al., 2018	GSE89728
WT stem cell TET1 CHIP-seq data	Dixon et al., 2021	GSE150072
Experimental models: Cell lines		
Human: HUES 8 hESC line (NIH approval number NIHhESC-09–0021)	HSCI iPS Core	hES Cell Line: HUES-8
Human: MEL-1 hESC line (NIH approval number NIHhESC-11–0139)	HSCI iPS Core	hES Cell Line: MEL-1
Human: H1 hESC line (NIH approval number NIHhESC-10–0043)	HSCI iPS Core	hES Cell Line: H1
HEK293T cell	ATCC	RRID:CVCL_0063
Oligonucleotides		
qPCR primers See Table S2.		N/A
CHIP-qPCR primers See Table S2.		N/A
Dox inducible construct		
BsiwI-NKX2–5 CDS-F	5'-TCATGA CGTACGatgttccccagccctgctct-3'	N/A
EcoRI-NKX2–5 CDS-R	5'-CTAGGAATTC ctaccaggctcggataccat-3'	N/A
BsiWI-TET1-F	5'ctgactcgtacgGC CACCATGGACTACAAGGACG-3'	N/A
AscI-TET 1-R	5'-ctgactGGCGCGCCTCAGACCCAATGGTTATAGG-3'	N/A
gRNAs targeting *NKX2–5* promoter		
5'-GACCAAAAAACGTTTCCCCC-3'	This paper	N/A
5'-GCCAGGTGGGCGGCAGAAAG-3'	This paper	N/A
5'-GTTTAGCTCTCAGGGAGGCG-3'	This paper	N/A
gRNAs targeting *TMEM88* promoter		
5'-AGGGCTCTGGTCCGCTCCT-3'	This paper	N/A
5'-TCCAGGGACCGCCCGTCGC-3'	This paper	N/A
5'-GGGCACAGCGAGCGGTTCC-3'	This paper	N/A
PCR-based bisulfite sequencing primers		
See Table S2		N/A
Recombinant DNA		
Plasmid: CS-TRE-NKX2–5-PRE-Ubc-tTA-I2G	This paper	N/A

REAGENT or RESOURCE	SOURCE	IDENTIFIER
Plasmid:CS-TRE-TET1-PRE-Ubc-tTA-I2G	This paper	N/A
Plasmid:pMuLE-Lenti-NKX2–5 gRNAs-mcherry-Neo	This paper	N/A
Plasmid:pMuLE-Lenti-TMEM88 gRNAs-mcherry-Neo	This paper	N/A
Plasmid: FH-TET1-pEF	Addgene	49792
Plasmid: dCas9-TET1CD lentiviral construct	Verma et al., 2018	N/A
Software and algorithms		
RRBSeeqer	Pan et al., 2015	https://icb.med.cornell.edu/wiki/index.php/Elementolab/RRBSseeqer_Tutorial
GREAT tool	McLean et al., 2010	http://great.stanford.edu/public/html/index.php
MEME Suite 5.5.5	McLeay and Bailey, 2010	https://meme-suite.org/meme/
Prism 7	Graphpad	N/A
bwa-0.7.17	Li and Durbin, 2009	http://bio-bwa.sourceforge.net/
macs14 1.4.2	Zhang et al., 2008	http://liulab.dfci.harvard.edu/MACS/00README.html